Title

Microcomposition of human urinary calculi using advanced imaging techniques.

Permalink

https://escholarship.org/uc/item/4291j8tt

Journal

Investigative urology, 189(2)

Authors

Flechner, Lawrence

Fakra, Sirine

Kahn, Arnold

et al.

Publication Date

2013-02-01

DOI

10.1016/j.juro.2012.09.098

Peer reviewed

Microcomposition of Human Urinary Calculi Using Advanced Imaging Techniques

Sarah D. Blaschko, **Joe Miller**, **Thomas Chi**, **Lawrence Flechner**, **Sirine Fakra**, **Arnold Kahn**, **Pankaj Kapahi**, and **Marshall L. Stoller**[*,†]

Department of Urology, University of California-San Francisco (SDB, JM, TC, LF, MLS), San Francisco, Advanced Light Source, Lawrence Berkeley National Laboratory (SF), Berkeley and Buck Institute for Research on Aging (AK, PK), Novato, California

Abstract

Purpose—Common methods of commercial urolithiasis analysis, such as light microscopy and Fourier transform infrared spectroscopy, provide limited or no information on the molecular composition of stones, which is vital when studying early stone pathogenesis. We used synchrotron radiation based microfocused x-ray fluorescence, x-ray absorption and x-ray diffraction advanced imaging techniques to identify and map the elemental composition, including trace elements, of urinary calculi on a μm (0.0001 cm) scale.

Materials and Methods—Human stone samples were obtained during serial percutaneous nephrolithotomy and ureteroscopy procedures. A portion of each sample was sent for commercial stone analysis and a portion was retained for synchrotron radiation based advanced imaging analysis.

Results—Synchrotron radiation based methods of stone analysis correctly identified stone composition and provided additional molecular detail on elemental components and spatial distribution in uroliths. Resolution was on the order of a few μm.

Conclusions—Knowledge of all elements present in lithogenesis at this detail allows for better understanding of early stone formation events, which may provide additional insight to prevent and treat stone formation.

Keywords

kidney; diagnostic imaging; nephrolithiasis; urolithiasis; radiography

Knowledge of stone composition directs urolithiasis treatment. However, most stones are calcium based and to our knowledge no marker exists to differentiate subtypes of these stones. As such, all calcium stones are approached in similar fashion surgically and therapeutically despite differences in composition. To better understand initial events in stone formation and determine optimal medical and surgical management of urolithiasis, a

[*]Correspondence: Department of Urology, University of California-San Francisco, 400 Parnassus Ave., A610, San Francisco, California 94143 (telephone: 415-476-1611; FAX: 415-476-8849; mstoller@urology.ucsf.edu).
[†]Financial interest and/or other relationship with Bard, Cook, Boston Scientific, EM Kinetics and Ravine Group.

more thorough knowledge of all elements present and their interactions are required. This information is not available using traditional stone analysis techniques.

Common methods of clinical stone analysis include in vivo imaging techniques, such as x-ray, ultrasound and CT, and ex vivo laboratory stone analyses, most commonly microscopy, FTIR and XRD. In vivo imaging alludes to stone composition and hardness by appearance on x-ray or by HU on CT but little additional information about stone composition can be ascertained. FTIR can determine stone composition and identify the proportions of constituents present in mixed composition stones. However, the accuracy of FTIR has been called into question.[1,2] The presence of trace elements and their location in the stone cannot be identified by FTIR or XRD.

Urolith morphology has been studied extensively with transmission electron microscopy and SEM.[3] Elemental composition can be determined with high precision and sensitivity using MS.[4] However, MS destroys the sample and does not provide information on the spatial distribution of elements. Elemental mapping has been performed using scanned electron[5] and proton beams,[6] which generate XRF radiation with element specific energy.

To our knowledge this study introduces a new type of advanced imaging technique to the urological community. It can identify the presence, location and chemical environment of elements, including trace elements, in uroliths with μm (10^{-6} m) resolution. An intense, tightly focused x-ray beam generated by a synchrotron particle accelerator is used as a probe and the emitted or transmitted x-rays are analyzed. The results of 5 stone samples are presented, and different analytical and imaging techniques are compared.

MATERIALS AND METHODS

Uroliths were obtained from human subjects during serial ureteroscopy and percutaneous nephrolithotomy procedures. Portions of the stones were sent for standard laboratory microscopic and FTIR analysis. Other samples were analyzed using synchrotron based μXRF, μXAS and μXRD at the Advanced Light Source beamline 10.3.2 in Berkeley, California. Examined stone samples included composite calcium phosphate, calcium oxalate, uric acid and cystine calculi (see table).

Fourier Transform Infrared Spectroscopy

Stones were analyzed at commercial laboratories by microscopic and FTIR identification. FTIR measures the absorption or emission of infrared light from a sample. The vibrational and rotational modes of atoms in a molecule can be excited by infrared radiation. Infrared absorption or emission can be used to study the nature of molecular bonds. Since different substances have distinct absorbance patterns and the degree of absorption is proportional to concentration,[7] FTIR can be used as a routine fingerprinting method by comparing measurements with known standards.[8] Unlike traditional spectroscopy, the main advantage of FTIR is that it simultaneously collects all frequencies in the infrared spectrum using a movable and a fixed mirror inside the interferometer, which significantly accelerates sample analysis. FTIR is the leading analytical technique for clinical laboratory kidney stone analysis.

X-Ray Fluorescence

XRF imaging uses an x-ray beam to ionize the atoms of a sample. The x-ray ionization process causes 1 inner shell electron of the atom to be emitted as a photoelectron, leaving an ion in an excited state and a core hole behind it. To relax to a lower energy state, an electron from an outer shell fills the core hole and the excess energy is emitted as fluorescence radiation (fig. 1). The energy of the emitted photons is the difference of the electron binding energies of the shells between which the transition occurred. Electron binding energies of various elements are different so that each atom can be identified uniquely. Furthermore, core shell ionization and relaxation are independent of valence electrons that form chemical bonds. Thus, atoms can be reliably identified in different molecular environments. However, this also means that XRF does not allow the study of interactions between atoms.

μXRF uses a microfocused x-ray beam with a focal spot of a few μm (fig. 2, *A*). The energy of the incoming x-ray radiation must be higher than the binding energy of the inner shell electrons for ionization to occur. This provides the flexibility to selectively ionize elements by choosing the appropriate x-ray energy. However, certain elements might be excluded by the limitations of the x-ray source. If the energy of emission lines of certain elements is closer than the energy resolution of the detector, these elements cannot be distinguished. The low energy cutoff of the x-ray detector (1,750 eV) limits the detection of elements to those with an atomic number of 14 or greater.

For all x-ray measurements stone samples were placed on Kapton® tape (which has negligible x-ray absorption) attached to an aluminum frame. Sample data were collected at room temperature. Cystine crystals were placed on molybdenum foil and mounted on a cooling stage. Data were collected at –30C. μXRF spectra were typically obtained in 30 to 40 seconds (fig. 3).

Synchrotron Radiation

X-ray generators are widely used in medicine. In an x-ray generator accelerated electrons hit a metal surface and ionize the atoms of the target. The subsequent relaxation process leads to the emission of characteristic x-rays, similar to fluorescence radiation, as described. The energy of this radiation depends on the target metal and can be changed only by replacing the target. This is not practical for routine medical or scientific applications.

Synchrotrons are another type of x-ray source based on particle accelerators, which were originally built for high energy physics experiments. A synchrotron is a circular accelerator with a diameter of tens to hundreds of meters. When a charged particle, eg an electron, is forced onto a circular path by a magnetic field in an accelerator, it emits SR. SR energy covers a broad range of the electromagnetic spectrum, including infrared, visible, ultraviolet, and soft and hard x-rays. SR is several orders of magnitude more intense than x-rays from a generator. It can be focused to a μm sized spot, while maintaining low divergence. SR from the accelerator is monochromatized by crystals and focused on a sample by mirrors. The collection of monochromator, mirrors, apertures and other components is called a beamline, which is typically tens of meters long and connects the exit port of the synchrotron to the sample area. The properties of SR, such as tunability and high brightness, make it an

indispensable tool for scientific research. Changing the x-ray energy enables the selective ionization of different electron shells and the high intensity allows the study of small samples. These unique capabilities created a new field of analytical techniques, including the elemental mapping of small specimens.

*μ*XRF Elemental Maps

A microfocused stationary x-ray beam with a sample mounted on an x-y stage enables the scanning of the surface of a sample. Collection of a *μ*XRF spectrum at each scan point yields an elemental map of the sample surface, which shows the spatial distribution of different atoms (fig. 4). Typically, a low resolution, coarse map is collected first with subsequent fine maps focusing on interesting areas. Data collection time is typically a few hours per map.

If *μ*XRF spectra or elemental maps are to be used for accurate quantitative analysis of sample composition, several points must be considered. The probability of the ionization of an atom depends on the x-ray energy and the core shell being ionized. These probabilities are known and tabulated in the literature. The emitted fluorescence intensity depends on the volume hit by the incoming beam. This can be calculated from the beam size and the penetration depth of the x-rays. Finally, self-absorption of emitted fluorescence by the sample must be considered. Absorption related complications can be overcome using thinly sliced samples, similar to those prepared for transmission electron microscopy.

*μ*XRF elemental mapping is possible with an x-ray generator. However, its flexibility is limited to the fixed x-ray energy and the significantly lower beam intensity, especially when focused on a small spot. XRF can also be generated through the impact of high energy electrons or protons on the sample. An SEM equipped with a fluorescence detector can also be used for elemental mapping.[5] The greatest advantage of an SEM is the high spatial resolution achievable (approximately 1 nm). However, extensive sample preparation, limited penetration depth of the electron beam (a few nm) and limited detection sensitivity from electron deceleration (bremsstrahlung) limits its usefulness. A PIXE instrument can also generate elemental maps with a reported beam spot size of 5 to 10 *μ*m if the proton beam is sufficiently focused.[6,9] PIXE requires sample preparation and beam penetration depth is a few *μ*m.

XAS and XANES

The *μ*XRF experiments described were performed with an x-ray beam at fixed energy while the energy of the emitted fluorescence radiation was analyzed. In an x-ray absorption experiment the energy of the x-ray beam was changed and the intensity of the beam transmitted through the sample was recorded (fig. 2, *B*). This type of experiment takes advantage of the energy tunability of x-rays from a synchrotron, which is not feasible with x-ray generators. The strongest absorption happens when the x-ray energy is near the ionization energy of an atomic shell because the x-ray photons are destroyed in the process. The ionization energy of an atomic shell is the same as the binding energy of the electrons in that shell. This is often called an absorption edge based on the shape of the absorption spectrum (fig. 5).

The near edge x-ray absorption spectrum of an element is influenced by the chemical state of the atom under investigation, and by the species, distances and chemical states of surrounding atoms. Modulations that arise in the absorption spectra are due to interactions of the emitted photoelectrons with neighboring atoms. Using this method, the oxidation state and coordination environment of atoms can be determined nondestructively.

Due to its sensitivity to the molecular environment, XANES is well suited to be a fingerprinting method. Using a database of previously measured spectra, the composition of samples can be accurately determined (fig. 5).

X-Ray Diffraction

In XRD an x-ray beam is focused at a sample. The periodicity of a crystalline structure causes interference effects, which results in a diffraction pattern (fig. 2, *C*). The diffraction pattern is characteristic and can be used as a fingerprint for matching against known patterns from a database.[8] Under the right circumstances the positions of all atoms in the sample can be determined without comparison to previously obtained structures. The greatest drawback of XRD is that the sample must be crystalline.

We performed μXRD using a microfocused x-ray beam, which allowed the diffraction analysis of small areas of our samples to investigate differences in composite stones (fig. 6). XRD experiments can be performed with laboratory based instruments based on x-ray generators. However, to achieve a small focal point of the x-ray beam for small samples or for spatial scanning, a high performance rotating anode generator with advanced optics is required.

Although XRD, XRF and elemental mapping can be done using smaller, separate, laboratory based instruments, XAS/XANES can only be performed using SR. SR also allows all techniques to be used on the same sample in short succession without further handling. Results can be combined in a meaningful way to guide subsequent testing.

Synchrotrons are large-scale scientific instruments that are built and operated at government research laboratories. The beamlines and end stations installed at synchrotrons are shared among many research groups. Access is limited, although it is free for approved academic researchers. For this reason, the SR based analytical methods described can be performed only intermittently. They are not suited for clinical analysis of a large number of stones on a regular basis.

RESULTS

Laboratory and synchrotron based methods of stone analysis were completed on mixed composition calcium oxalate, calcium phosphate, uric acid and cystine stones. The results of x-ray analysis techniques were concordant with those of commercial FTIR (see table).

Fourier Transform Infrared Spectroscopy

FTIR results included information on stone type and the percent of different components in mixed composition stones (see table). No information was provided on trace elements.

Microfocused XRF

*µ*XRF measurements were made on all samples. Various x-ray energies were used to distinguish among the K-shells of different elements. In the fluorescence spectra of the cystine stone sulfur is the dominant emission peak. For calcium based stones the calcium peak dominates and for calcium phosphate stones phosphorus is also strongly present (fig. 3).

The sensitivity of *µ*XRF allowed trace elements to be identified in all samples (see table). All stones contained small amounts of iron, zinc, chlorine and potassium. Sample 1 contained lead, whereas the cystine sample contained small amounts of copper and chromium. Calcium based stones also contained strontium, which is known to incorporate into calcifying structures and tissues.[10–12]

Composite sample 1 had a strong phosphorus signal in the calcium phosphate region, a weak phosphorus signal at a border zone and no phosphorus signal in the calcium oxalate portion of the stone. Sample 3, a composite stone, also demonstrated a strong phosphorus peak in the calcium phosphate area (see table).

XRF Elemental Maps

Calcium *µ*XRF maps demonstrated a strong calcium signal across all calcium based samples (fig. 4). Sample 3, a uric acid/calcium composite stone, had an uneven calcium distribution. The upper and lower edges clearly contained more calcium than the central part (fig. 4, *B*, arrows). This indicates the specific micro architecture of this sample, where the localization of the calcium oxalate/calcium phosphate portion on the edges can be distinguished from the uric acid portion in the middle.

Due to the experimental geometry used for *µ*XRF mapping (fig. 2, *A*), the surface topography of samples can result in absorption of the emitted fluorescence radiation. This causes intensity variations (shadows) in the signal, which must be considered when interpreting elemental distributions (fig. 4).

X-Ray Absorption Near Edge Structure

Calcium *µ*XANES spectra were collected at multiple locations of stones containing calcium phosphate and calcium oxalate components (see table). Using *µ*XANES as a fingerprinting method and comparing our results to a database of XANES spectra, calcium oxalate and hydroxyapatite were identified (fig. 5).

X-Ray Diffraction

*µ*XRD measurements were performed on calcium phosphate stone and used as a fingerprinting method. Diffraction patterns were compared to known patterns. An excellent match was found for hydroxyapatite (fig. 6).

DISCUSSION

All analytical methods used in the current study yielded consistent results, validating the newly introduced microfocused x-ray beam techniques as an excellent tool for investigating renal stone formation. These x-ray techniques enabled high resolution imaging of uroliths, determination of chemical composition and detection of numerous trace elements that are integral parts of kidney stones. The study of these trace elements, particularly zinc, and their pivotal role in stone formation is promising (Chi et al, unpublished data).

All stone analysis methods have limitations. Gross examination and light microscopy may provide sufficient topographic information for the preliminary identification of characteristic pure stones but they cannot consistently identify composite stones. The constituents of composite stones can be determined by FTIR but the presence of trace elements and the spatial distribution of elements cannot be determined. XRD provides elemental composition but cannot evaluate amorphous materials, such as matrix stones. MS can identify elemental composition and trace elements but the sample is vaporized during evaluation so that elemental spatial distribution cannot be evaluated. Electron microscopy provides high spatial resolution but no information on the elemental or molecular composition of samples (see Appendix).

The integrated experimental setup that we used allowed us to perform μXRF, μXAS and μXRD measurements in short succession without removing samples from the mounting. Thus, the advantages of all 3 methods could be exploited by combining sensitive elemental and chemical composition measurements with μm scale imaging.[13] The microfocused x-ray beam necessary for these experiments is made possible by the unique properties of SR, including energy tunability, low divergence and high intensity.

Recent advances in stone composition specific therapy have been enabled by detailed knowledge of stone formation and composition. For example, the administration of methylated cystine interrupts the normal crystallization of cystine stones.[14] Moreover, cystine stones have differing susceptibility to lithotripsy based on their relative roughness or smoothness, suggesting differences in crystallization.[15] On the other hand, the lower amount of trace elements in calcium oxalate monohydrate stones makes them more resistant to lithotripsy.[16] Additional focus has been placed on identifying the trace elements involved in lithogenesis and the role that these elements may have in stone formation.[10–12] SR techniques provide detailed data on the presence and interactions of elements in uroliths that are not available using other analytical techniques.

CONCLUSIONS

Only the advanced imaging techniques used in this study allow for the identification and spatial resolution of trace elements in stones. Since no new urolithiasis medications have been developed in approximately 20 years, additional information about elemental interactions in stones is clearly needed for drug discovery. Knowledge of trace elements that augment stone formation or make stones more resistant to lithotripsy may lead to the development of directed chelators or the modification of trace elements to help prevent stone

formation or cause the formation of stones that are more easily fragmented. Identifying trace elements and their interactions in stones may be essential for urolithiasis treatment. Until we better understand stone composition, we will make little headway in improving stone therapy and initiating preventive measures against stone formation.

Acknowledgments

Abbreviations and Acronyms

μXANES	micro-XANES
μXAS	microfocused XAS
μXRD	microfocused XRD
μXRF	microfocused XRF
CT	computerized tomography
FTIR	Fourier transform infrared spectroscopy
MS	mass spectroscopy
PIXE	proton induced x-ray emission
SEM	scanning electron microscopy
SR	synchotron radiation
XANES	x-ray absorption near edge structure
XAS	x-ray absorption
XRD	x-ray diffraction
XRF	x-ray fluorescence

References

1. Hesse A, Kruse R, Geilenkeuser WJ. Quality control in urinary stone analysis: results of 44 ring trials (1980–2001). Clin Chem Lab Med. 2005; 43:298. [PubMed: 15843235]

2. Krambeck AE, Lingeman JE, McAteer JA. Analysis of mixed stones is prone to error: a study with US laboratories using micro CT for verification of sample content. Urol Res. 2010; 38:469. [PubMed: 20967439]

3. Khan SR. Calcium phosphate/calcium oxalate crystal association in urinary stones: implications for heterogeneous nucleation of calcium oxalate. J Urol. 1997; 157:376. [PubMed: 8976301]

4. Hesse A, Dietze HJ, Berg W, et al. Mass spectrometric trace element analysis of calcium oxalate uroliths. Eur Urol. 1977; 3:359. [PubMed: 604069]

5. Khan SR, Hackett RL. Identification of urinary stone and sediment crystals by scanning electron microscopy and x-ray microanalysis. J Urol. 1986; 135:818. [PubMed: 3959214]

6. Pineda CA, Rodgers AL, Prozesky VM, et al. Elemental mapping analysis of recurrent calcium oxalate human kidney stones. Nucl Instrum Methods Phys Res B. 1995; 104:351.

7. Griffiths, P.; de Hasseth, JA. Fourier Transform Infrared Spectrometry. 2. Hoboken: John Wiley & Sons; 2007.

8. Mandel, I.; Mandel, N. Structure and compositional analysis of kidney stones. In: Stoller, ML.; Meng, MV., editors. Urinary Stone Disease: The Practical Guide to Medical and Surgical Management. Totowa, New Jersey: Humana Press; 2007. p. 69-81.

9. Pineda CA, Peisach M. Micro-analysis of kidney stones sequentially excreted from a single patient. Nucl Instrum Methods Phys Res B. 1994; 85:896.

10. Singh VK, Rai AK, Rai PK, et al. Cross-sectional study of kidney stones by laser-induced breakdown spectroscopy. Lasers Med Sci. 2009; 24:749. [PubMed: 19104906]

11. Bazin D, Carpentier X, Brocheriou I, et al. Revisiting the localisation of Zn(2+) cations sorbed on pathological apatite calcifications made through X-ray absorption spectroscopy. Biochimie. 2009; 91:1294. [PubMed: 19497348]

12. Carpentier X, Bazin D, Combes C, et al. High Zn content of Randall's plaque: a μ-X-ray fluorescence investigation. J Trace Elem Med Biol. 2011; 25:160. [PubMed: 21763116]

13. Marcus MA, MacDowell AA, Celestre R. Beamline 10.3. 2 at ALS: a hard X-ray microprobe for environmental and materials sciences. J Synchrotron Radiat. 2004; 11:239. [PubMed: 15103110]

14. Rimer JD, An Z, Zhu Z, et al. Crystal growth inhibitors for the prevention of L-cystine kidney stones through molecular design. Science. 2010; 330:337. [PubMed: 20947757]

15. Bhatta KM, Prien EL Jr, Dretler SP. Cystine calculi—rough and smooth: a new clinical distinction. J Urol. 1989; 142:937. [PubMed: 2795746]

16. Turgut M, Unal I, Berber A, et al. The concentration of Zn, Mg and Mn in calcium oxalate monohydrate stones appears to interfere with their fragility in ESWL therapy. Urol Res. 2008; 36:31. [PubMed: 18176803]

Appendix

APPENDIX

Experimental stone analysis techniques according to spatial resolution

Method (characteristics)	Spatial Resolution (nm)	Advantages	Disadvantages	Description
FTIR* (spectroscopic, laboratory + synchrotron based, transmission)	Not applicable	Mature technique, available at many laboratories, inexpensive, determines sample molecular composition	No elemental composition	Infrared spectroscopy excites molecular bond vibrational + rotational modes, detecting specific bond types, eg C-C, C-O
MS (spectroscopic, laboratory based)	Not applicable	Mature technique, available at many laboratories, sensitive + accurate composition determination, including atoms, molecules + fragments	Sample is vaporized	Measures charged particle mass-to-charge ratio
Transmission electron microscopy (imaging,	Greater than 0.2	Highest spatial resolution	No elemental mapping, large, expensive, extensive sample	Contrast originates from

Method (characteristics)	Spatial Resolution (nm)	Advantages	Disadvantages	Description
diffractive, laboratory based, transmission)		analytical technique, diffraction + elemental analysis possible	preparation, limited sample types	differences in electron absorption electrons through thin sample
SEM (imaging, diffractive, laboratory based, reflection)	Greater than 1	High spatial resolution, elemental mapping (Z greater than 5) + diffraction possible	Typically sample preparation is necessary, large, expensive	Secondary electrons reflected from sample surface provide topology. Adding XRF detector enables elemental determination/ mapping
Scanning transmission x-ray microscopy (imaging, spectroscopic, synchrotron based, transmission)	Greater than 10	μXAS with high spatial resolution yields elemental maps + chemical environment information	Synchrotron based, not easily accessible, thinly sectioned samples needed	X-ray absorption is measured through thin sample + x-ray energy tunability yields elemental sensitivity
Bright field microscopy/ light microscopy[*] (imaging, laboratory based, transmission, reflection)	Greater than 200	Easily accessible, inexpensive, stereo microscope gives 3D image	Information limited by magnification + visible light use	Contrast originates from visible light absorption/ reflection differences
MicroCT (imaging, laboratory and synchrotron based, transmission)	Greater than 200	Lab based, medium sized, non destructive, yields 3-dimensional image of sample internal structure	No elemental composition, expensive	Contrast originates from x-ray absorption differences
PIXE, microPIXE	Greater than 1,000	Provides elemental composition (Z greater than 11), can detect trace elements with high sensitivity on absolute scale, spatial elemental mapping possible with microfocused beam	Large, expensive, sample preparation needed	Sample irradiation with high energy protons leads to XRF radiation emission, of which energy is element specific
XAS, extended x-ray absorption fine structure, XANES, μXAS,[*] micro-extended x-ray absorption fine structure, μXANES (spectroscopic,	Greater than 2,000	Can determine chemical environment of specific elements	Synchrotron based	X-ray absorption is measured over small x-ray energy range near absorption edge

Method (characteristics)	Spatial Resolution (nm)	Advantages	Disadvantages	Description
synchrotron based, transmission, reflection)				
XRF, μXRF[*] (imaging, spectroscopic, laboratory + synchrotron based, reflection)[†]	Greater than 2,000	Provides elemental composition (Z greater than 13), can detect trace elements, laboratory based instruments common, spatial elemental mapping possible at synchrotron with microfocused beam	No information on element molecular environment, high resolution elemental mapping requires synchrotron	Sample x-ray irradiation leads to fluorescence radiation emission, of which energy is element specific
XRD, μXRD[*] (diffractive, laboratory + synchrotron based, transmission)	Greater than 2,000	Mature technique, available at many laboratories, can accurately determine crystalline material composition	Sample must be in crystal form, high intensity microfocused beam requires synchrotron	Crystalline material diffraction pattern provides crystal fingerprinting or 3-dimensional atomic structure

[*] Technique was used in study.

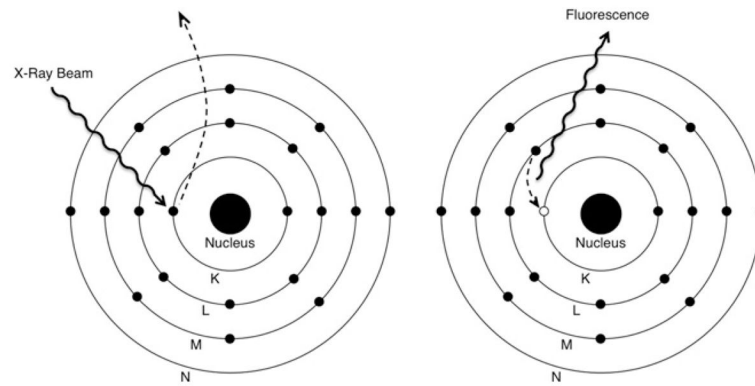[†] For electron and proton induced XRF see SEM and PIXE.

Figure 1.
XRF in calcium. Incoming x-ray photon excites core shell electron of atom, in this case K-shell electron. Core hole is filled by 1 outer electron and extra energy, which is binding energy difference of 2 shells, is released as fluorescence radiation. Since electron binding energies are element specific, analyzing fluorescence energy can be used to determine atomic composition of its source. Calcium photoionization and subsequent fluorescence emission shown resulted in calcium K peak of 3,690 eV energy (K and L electron binding energies were 4,038.5 and 348.5 eV, respectively). To generate calcium K peak energy of incoming x-ray beam must be higher than 4,038.5 eV (fig. 3). X-ray emission peaks are labeled based on shell from which they originated. *L*, *M* and *N*, electron shells.
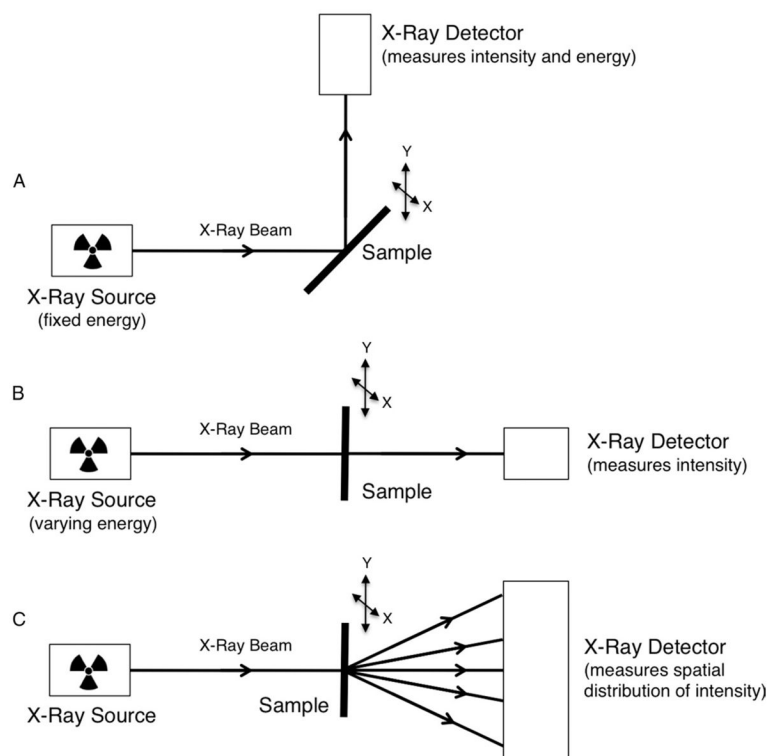
Figure 2.
Some analytical methods used for stone analysis. *A*, typical *μ*XRF measurement setup. Focused (few *μ*m in diameter) x-ray beam of single energy hits sample mounted on x-y stage. Emitted fluorescence is detected and energy is analyzed in x-ray detector. As stage is scanned, elemental map of sample can be generated. *B*, transmission of x-ray beam of varying energy through sample is measured in XAS experiment. Microfocused beam and x-y stage enable spectroscopy on different parts of sample (*μ*XAS). *C*, XRD occurs in crystalline samples where monochromatic x-ray beam generates diffraction pattern, which is recorded on detector with large surface area. Microfocused beam and x-y stage enable diffraction measurements on different parts of sample (*μ*XRD).
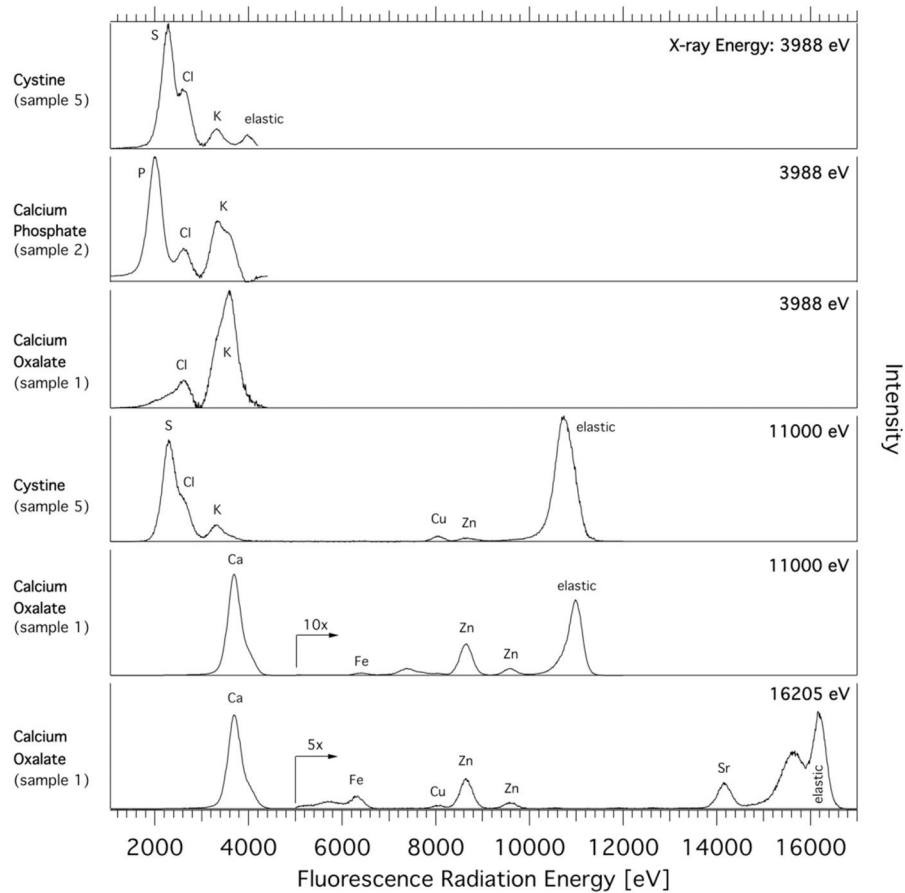
Figure 3.
XRF spectra of representative stone samples collected at 3 x-ray energies. Calcium containing stones showed strong calcium K peak at 3,690 eV as long as exciting x-ray energy was above K-shell ionization threshold, also known as K-edge, of 4,038.5 eV. Second and third spectra showed no calcium signal because x-ray excitation energy was below calcium core shell ionization energy, thus, deliberately excluding calcium measurement. Purpose was to see signal from other elements, such as phosphorus for apatite stone, which would be masked by strong calcium peak. Cystine sample shows strong sulfur K peak. Due to μXRF method high sensitivity, trace elements chlorine, potassium, iron, zinc, copper and strontium were also observed. Elastic peak represents incoming x-ray beam, which was scattered without energy loss.
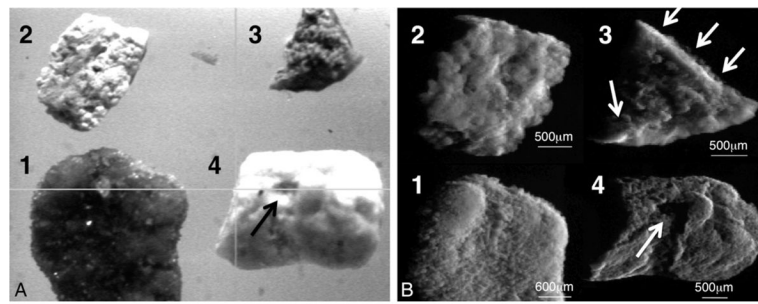
Figure 4.
A, detailed image of stone samples mounted on beamline x-y stage. *B*, *μ*XRF elemental maps reveals calcium distribution with image brightness proportional to calcium signal strength. Data were collected at 1,6205 eV x-ray energy, 20 *μ*m pixel size and 15 × 6 *μ*m beam spot size. Left edge shows weaker calcium fluorescence signal for all 4 maps due to shadowing effect caused by experimental geometry. Similarly, signal from indentation (arrow) in sample 4 was weakened by protrusion at right. Sample 3 was composite stone (see table), resulting in uneven calcium distribution. Note strong calcium signal on upper and lower edges (arrows). Scale bars indicate 600 (sample 1) and 500 (samples 2 to 4) *μ*m.
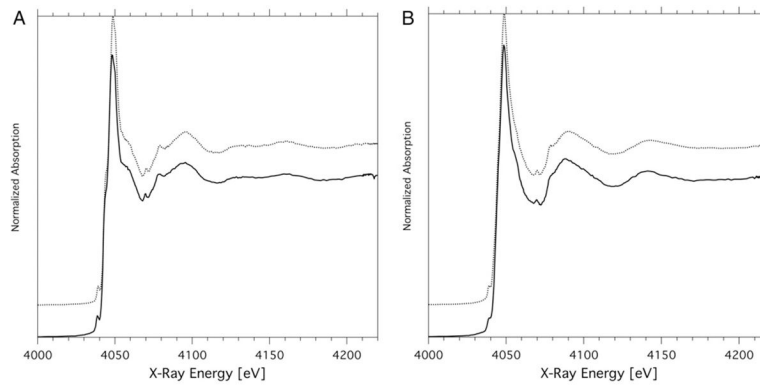
Figure 5.
Calcium XANES spectra (solid lines) of composite stone sample 3 containing hydroxyapatite and calcium oxalate. For calcium innermost absorption edge (K-edge) occurred at 4,038.5 eV. Data were collected with 9×3 μm beam at 2 distinct stone portions. XANES spectra from calcium compound library were compared to our measurements for compound identification (dotted lines). *A*, hydroxyapatite stone portion. *B*, calcium oxalate stone portion.
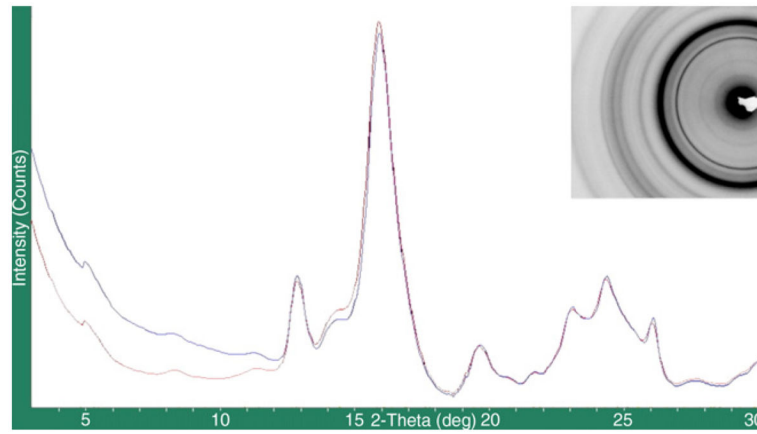
Figure 6.
μXRD of calcium phosphate stone sample 4. Two distinct locations of same sample were analyzed by focused x-ray beam with 15×6 μm spot size and 16,000 eV energy. Inset, powder diffraction pattern corresponding to blue curve. Diffraction intensity for each site matched hydroxyapatite diffraction.

Table 1

Composition of study samples on commercial FTIR and synchrotron based techniques

Sample No.[*]	FTIR Composition (%)	μXRF (No. sites)	Calcium μXANES (No. sections)
1	Calcium oxalate dihydrate (15), calcium oxalate monohydrate (70), calcium phosphate (15)	Calcium, iron, zinc, strontium, potassium, chlorine, lead, phosphorus (1), calcium, iron, zinc, strontium, potassium, chlorine (1), calcium, iron, zinc, strontium, potassium, chlorine (1)	Calcium oxalate (1), hydroxyapatite (1)
2	Calcium phosphate (90), calcium oxalate dihydrate (10)	Calcium, iron, zinc, strontium, potassium, chlorine, phosphorus	Hydroxyapatite
3:			
Subsection 1	Uric acid (80), ammonium acid urate (20)	Calcium, iron, zinc, strontium, potassium, chlorine, phosphorus	
Subsection 2	Calcium oxalate monohydrate (80), calcium phosphate (20)		Calcium oxalate (1), hydroxyapatite (1)
4[†]	Calcium phosphate (100)	Calcium, iron, zinc, strontium, potassium, chlorine, phosphorus (2)	
5	Cystine (100)	Sulfur, iron, zinc, potassium, chlorine, copper, chromium	

[*] Typically several sites were probed per sample using microfocused x-ray beam. Calcium XANES measurements were performed on sample thin sections and all other data were collected on bulk stones (figs. 3 and 5).

[†] On μXRD hydroxyapatite $\times$ 2.